Numerical Study of Vertical Shear and Stratification Effects on the Evolution of a Vortex Pair

Robert E. Robins* and Donald P. Delisi†
Northwest Research Associates, Inc., Bellevue, Washington

The objective of this study is to investigate with a numerical model how coexisting vertical shear and stratification affect the evolution of a vortex pair. Our results show that the Richardson number (the ratio of stratification forces to shear forces) is an important parameter in the evolution. When the Richardson number is large, the vortex pair evolves more or less symmetrically, the left and right vortex decaying equally, or nearly equally, rapidly. In this case, the effect of the shear is small, and stratification dominates the evolution. When the Richardson number is sufficiently small, however, the evolution is dramatically different. Under these conditions, the vortices evolve asymmetrically, and the vortex with rotational sense opposite to that of the mean shear decays while the vortex with the same rotational sense as the mean shear survives. This "solitary vortex" then decays slowly with time. The transition from solitary to nonsolitary vortex evolution occurs over Richardson numbers between 0.5 and 4 for the Froude number range 0.5 to 4.0.

Nomenclature

B_0 = circulation parameter, = circulation/2π
b_0 = half separation of vortex pair
F_M = ideal vortex migration Froude number, $V_m/2b_0N_0$
F_r = vortex migration Froude number, $V_0/2b_0N_0$
F_S = shear parameter, $V_M/2b_0U_z$
F_T = nondimensional parameter, U_0T_0/L_0, which = 1
g = gravitational acceleration
H = vortex pair rise height
L = width of computational domain
L_0 = scaling length, $2b_0$
N_0 = Brunt-Vaisala frequency
Pr = Prandtl number, ν/κ
Re = Reynolds number, B_0/ν
Ri = Richardson number, N_0^2/U_z^2
R_0 = scaling density, $\rho_0N_0^2L_0/g$
r_c = nondimensional core size parameter, $r_0/2b_0$
r_0 = vortex core size parameter
T_0 = scaling time, L_0/U_0
t = time
$\bar{t}$ = nondimensional time, t/T_0
U = horizontal speed of background fluid
U_z = vertical shear of background fluid, dU/dz
U_0 = perturbation scaling speed, $B_0/2b_0$
$\bar{U}_0$ = mean scaling speed, $2b_0U_z$
u = horizontal speed, $-\partial\psi/\partial z$
V_M = ideal vortex pair rise rate, $B_0/2b_0$
V_0 = measured vortex pair rise rate
w = vertical speed, $\partial\psi/\partial x$
x = horizontal coordinate
z = vertical coordinate
η = vorticity
$\bar{\eta}$ = mean vorticity
η' = perturbation vorticity
η'_0 = initial perturbation vorticity
κ = mass diffusivity
ν = kinematic viscosity
ρ = density
$\bar{\rho}$ = mean density
ρ' = pertubation density
ρ_0 = reference density
ψ = stream function (see u and w)
$\bar{\psi}$ = mean stream function
ψ' = perturbation stream function

Received Oct. 25, 1988; revision received June 12, 1989.

*Research Scientist. Member AIAA.
†Senior Research Scientist. Member AIAA.

I. Introduction

THE evolution, persistence, and breakdown of vortices have received much attention in aerodynamics. A large impetus to these studies has been aircraft trailing vortices, as they are hazards to following aircraft and thus are an important factor in determining airport capacity.[1] Measurements of these aircraft trailing vortices have been reported by several authors.[2-8] In most of these studies, a tilting of the vortex pair has been frequently seen, and, sometimes, solitary vortices have been observed to emerge. These solitary vortices have been observed to persist for much longer times than vortex pairs. It has been suggested[6] that vertical shear is a key element in the occurrence of vortex pair tilting and the emergence of solitary vortices.

There have been many other previously reported studies of vortex evolution. Numerically, Hill[9] studied the descent of a vortex pair in a stratified, nonsheared environment; Hecht et al. compared numerical solutions to their vortex ring experiments[10] and to observations of trailing tip vortices from a Boeing 747 aircraft[11]; and Sarpkaya and Johnson[12] compared numerical simulations to their experimental observations. Analytically, Crow[13] reported on the sinusoidal instability of a vortex pair in a nonstratified, nonsheared fluid, and Scorer and Davenport,[14] Saffman,[15] Crow,[16] and Greene[17] examined vortex evolution in a stratified, nonsheared environment. Experimentally, in nonstratified, nonsheared flows, Olsen[18] performed flow visualization studies of trailing-tip vortices from airfoils. Baker et al.[19] used a laser-Doppler velocimeter to measure velocity profiles behind airfoils, Maxworthy[20] measured vortex rings (including some qualitative observations of experiments in stratified flows), and Barker and Crow[21] performed measurements on two-dimensional vortex pairs. In stratified, nonsheared fluids, Tomassian[22] essentially repeated Barker and Crow's measurements in a stratified fluid away from a ground plane, Hecht et al.[10] measured vortex rings, and Sarpkaya and Johnson[12] and Sarpkaya[23] measured trailing-tip vortices from airfoils. Reviews of vortex dynamics and breakdowns have also been given.[24-28]

None of the preceding studies include shear effects. (Whenever we refer to shear we mean vertical shear, i.e., a

change in the horizontal wind speed as a function of the vertical coordinate.) The only vortex studies known to us which include the effects of shear are numerical calculations reported by Rossow[29] and Bilanin et al.,[30] and neither of those studies included stratification. The results of those studies showed that shear can have significant effects on vortex evolution: the vortex with the same rotational sense as the shear survives, and the other vortex decays. The question left unanswered by their studies is how shear and stratification together affect vortex evolution.

To date, no studies of vortex evolution have been reported in a sheared and stratified flow. Real geophysical fluids are, in general, however, both sheared and stratified. The ratio of buoyancy forces to inertial, or shear, forces is characterized by the Richardson number

$$Ri = \frac{N_0^2}{(\mathrm{d}U/\mathrm{d}z)^2} \tag{1}$$

where

$$N_0 = \left(-\frac{g}{\rho}\frac{\mathrm{d}\rho}{\mathrm{d}z} \right)^{1/2}$$

is the Brunt-Vaisala (B-V) frequency ($2\pi/N_0$ is the B-V period). Recent measurements in the ocean[31-33] and in the atmosphere[34-36] suggest that the Richardson number is commonly of order unity, indicating that the effects of shear are of the same order of magnitude as the effects of stratification. Thus, the realistic modeling of vorticies in geophysical fluids requires that both shear and stratification be included in the flow.

In this paper, we use a numerical model to examine the evolution of a vortex pair far from a ground plane in flows where the Richardson number is varied between zero and infinity. The objective of this initial study is to try to define the parameter range of interest. Our results are significant for two reasons: First, our results bridge the gap between earlier studies with stratification but no shear ($Ri = \infty$) and studies with shear but no stratification ($Ri = 0$). We thus present results of vortex evolution in a geophysically relevant but previously unexplored flow regime. Second, we will show that the evolution of a vortex pair in sheared flows, is, under certain conditions, dramatically different from that in nonsheared flows and that a solitary vortex emerges when the Richardson number is of order unity or less. The solitary vortex regime appears to be distinct, and once developed, a solitary vortex appears to decay slowly. Thus, we show that the fate of a vortex pair is highly dependent on the ambient Richardson number.

Of course, there are factors other than vertical shear and stratification which affect the fate of aircraft trailing vortices. Ambient turbulence and ground interaction should also be considered as should vortex generated turbulence, vortex filament linking due to mutual induction, and vortex breakdown due to core bursting. However, since no previous study has considered the combined effect of vertical shear and stratification, we feel justified in reporting on an idealized problem.

In Sec. II, we present the details of our numerical model. In Sec. III, we compare vortex rise rates computed from this model with previously reported laboratory observations in stratified and nonstratified, but nonsheared, flows. In Sec. IV, we show the evolution of a vortex pair in stratified flows, and show how background shear effects the evolution. Further results and a discussion are presented in Sec. V.

II. Numerical Model

The numerical results described in this study were obtained from a numerical model originally developed for use in gravity wave-critical level studies.[37-40] The model solves the two-dimensional, time-dependent Navier-Stokes equations, expressed in stream-function-vorticity form, to which a Boussinesq approximation (density variations in the momentum equations are neglected except where they give rise to buoyancy forces) has been applied. These equations, expressed in dimensional form, are as follows:

$$\frac{\partial \eta}{\partial t} + J(\psi,\eta) - \frac{g}{\rho_0}\frac{\partial \rho}{\partial x} - \nu\nabla^2\eta = 0 \tag{2}$$

$$\frac{\partial \rho}{\partial t} + J(\psi,\rho) - \kappa\nabla^2\rho = 0 \tag{3}$$

$$\nabla^2\psi = -\eta \tag{4}$$

Here ψ is a stream function defined by

$$u = -\frac{\partial \psi}{\partial z} \text{ and } w = \frac{\partial \psi}{\partial x} \tag{5}$$

The Jacobian operator $J(f,h)$ is defined by

$$J(f,h) = \frac{\partial f}{\partial x}\frac{\partial h}{\partial z} - \frac{\partial h}{\partial x}\frac{\partial f}{\partial z} \tag{6}$$

where f and h are symbolic functions.

The model obtains separate solutions for horizontally averaged quantities and for the perturbations about these averages. No assumptions are made in the model about the size of the perturbations. The equations governing the horizontal mean and perturbation quantities, in nondimensional form, are as follows:

$$\frac{\partial \bar{\eta}}{\partial t} + F_T F_S \overline{J(\psi',\eta')} - \frac{F_T}{Re}\frac{\partial^2}{\partial z^2}\bar{\eta} = 0 \tag{7}$$

$$\frac{\partial \bar{\rho}}{\partial t} + F_T \overline{J(\psi',\rho')} - \frac{F_T}{PrRe}\frac{\partial^2}{\partial z^2}\bar{\rho} = 0 \tag{8}$$

$$\frac{\partial^2 \bar{\psi}}{\partial z^2} = -\bar{\eta} \tag{9}$$

$$\frac{\partial \eta'}{\partial t} - \frac{F_T}{F_S}\left(\frac{\partial \bar{\psi}}{\partial z}\frac{\partial \eta'}{\partial x} - \frac{\partial \bar{\eta}}{\partial z}\frac{\partial \psi'}{\partial x} \right) + F_T[J(\psi',\eta') - J(\psi',\eta')]$$

$$- \frac{1}{F_T F_M^2}\frac{\partial \rho'}{\partial x} - \frac{F_T}{Re}\nabla^2\eta' = 0 \tag{10}$$

$$\frac{\partial \rho'}{\partial t} - F_T\left(\frac{1}{F_S}\frac{\partial \bar{\psi}}{\partial z}\frac{\partial \rho'}{\partial x} - \frac{\partial \bar{\rho}}{\partial z}\frac{\partial \psi'}{\partial x} \right) + F_T[J(\psi',\rho') - \overline{J(\psi',\rho')}]$$

$$- \frac{F_T}{PrRe}\nabla^2\rho' = 0 \tag{11}$$

$$\nabla^2\psi' = -\eta' \tag{12}$$

where overbars indicate horizontal mean quantities and primes denote perturbations. Nondimensional parameters are

$$Re = \frac{U_0 L_0}{\nu} \tag{13}$$

$$Pr = \frac{\nu}{\kappa} \tag{14}$$

$$F_M^2 = \frac{\rho_0 L_0}{g R_0 T_0^2} \tag{15}$$

$$F_S = \frac{U_0}{\bar{U}_0} \tag{16}$$

$$F_T = \frac{U_0 T_0}{L_0} \tag{17}$$

where F_M, F_S, and F_T will be further identified when values for the various scales are chosen.

The solution method is to represent the horizontal variation of the three perturbation quantities in terms of complex exponential series with coefficients depending on z and t. Side boundaries are thus periodic, and top and bottom boundaries are chosen to be rigid and free slip. Centered differences are used to approximate vertical derivatives of mean and perturbation quantities, and a leap-frog scheme is used to advance the solution in time. To enhance the numerical stability of the scheme, difference approximations to second derivatives are computed on a forward-time basis,[41] and results from successive time steps are periodically averaged.

The numerical vortices used in this study are specified as an initial field of perturbation vorticity. The defining expression in dimensional form is

$$\eta_0'(x,z) = \frac{2B_0}{r_0^2} \exp - (z/r_0)^2 \, [\exp - (x - b_0/r_0)^2 - \exp - (x + b_0/r_0)^2] \tag{18}$$

where $2B_0\pi$ is the circulation associated with each of the vortices, r_0 determines their radial extent, and $2b_0$ is their separation. This specification results in a vortex pair having an initial vertical migration rise rate which tends to $V_M = B_0/2b_0$ as r_0 tends to zero.

The properties of the fluid in which the vortices evolve are specified by vertical profiles of mean density and wind. The model does not restrict the form of these profiles, except that model results will become chaotic if unstable stratification conditions are specified. For the calculations reported here, we have used profiles with stable uniform density gradient and uniform shear.

If we represent the uniform shear by U_z, then convenient choices for the scaling parameters are $T_0 = L_0/U_0$, $L_0 = 2b_0$, $U_0 = B_0/2b_0$, $\bar{U}_0 = U_z(2b_0)$, and $R_0 = \rho_0 N_0^2 L_0/g$. With these choices, the nondimensional parameters, defined in Eqs. (13–17), become

$$Re = \frac{B_0}{\nu} \tag{19}$$

$$Pr = \frac{\nu}{\kappa} \tag{20}$$

$$F_M = \frac{B_0}{N_0(2b_0)^2} = \frac{V_M}{N_0(2b_0)} \tag{21}$$

$$F_S = \frac{B_0}{U_z(2b_0)^2} = \frac{V_M}{U_z(2b_0)} \tag{22}$$

$$F_T = 1 \tag{23}$$

where V_M is the ideal vortex migration rate defined by $B_0/2b_0$. Here, F_M is the ideal vortex migration Froude number and is the ratio of the inertia force of the vortex pair to the buoyancy force exerted by the stratification on the vortices. The F_S is a shear parameter and is analogous to F_M; F_M and F_S can be thought of as characterizing the intensity of the vortices relative to stratification and shear, respectively. The Richardson number is given by $Ri = N_0^2/U_z^2 = F_S^2/F_M^2$. The initial field of perturbation vorticity, given by Eq. (18), can now be written in nondimensional form as

$$\eta_0'(x,z) = \frac{2}{r_c^2} \exp[-(z/r_c)^2] \, \{\exp[-(x - 0.5)^2/r_c^2] - \exp[-(x + 0.5)^2/r_c^2]\} \tag{24}$$

where the nondimensional parameter r_c is $r_0/2b_0$.

To prevent the buildup of excessive energy at small scales of motion, we adopted a wave-number-dependent damping model. To describe the damping model, we first write down the series representation for the Laplacians appearing in the diffusion terms of Eqs. (10) and (11). Letting $\phi' = \eta'$ or ρ', we have

$$\nabla^2\phi' = \sum_{\substack{n=-N \\ n\neq 0}}^{N} D_n(z,t)e^{i\alpha nx}, \quad \alpha = \frac{2\pi}{L} \tag{25}$$

where

$$D_n(z,t) = \left(\frac{\partial^2}{\partial z^2} - \alpha^2 n^2\right) \phi_n(z,t) \tag{26}$$

the functions ϕ_n being the coefficients in the series representation of ϕ'. The damping approach used in the model is to include, on the left side in Eqs. (10) and (11), a diffusion-like term of the form

$$D(x,z,t) = -\frac{D_0}{Re} \sum_{\substack{n=-N \\ n\neq 0}}^{N} d_n D(z,t)e^{i\alpha nx} \tag{27}$$

where d_n depends only on n ($d_{-n} = d_n$). The $D(x,z,t)$ is, in fact, a generalization of the diffusion terms appearing in Eqs. (10) and (11); e.g., it is identical to the molecular diffusion term when $d_n = 1$ for all n, and $D_0 = 1$. All we require to specify the damping model completely are choices for D_0 and d_n.

In order to damp out only small scale (large n) components of the solution, we choose d_n as follows:

$$d_n = 0.5\left(1 + \tanh\frac{n - n^*}{\Delta n}\right) \tag{28}$$

where n^* denotes the midpoint of the transition from undamped to damped solution components, and Δn specifies the rate of the transition (smaller Δn implies more rapid transition). The quantity D_0 is chosen to be as large as necessary to make the damping effective (see below).

In practice, the damping introduced by this model appears to have a minimal effect on the dynamics of flows whose energy is concentrated in harmonics 1 through n, where $n < n^* - \Delta n$. To illustrate this point, we calculated the evolution of a laboratory-scale vortex pair in a nonstratified, nonsheared fluid, which we took to be water. Thus, $\rho_0 = 1000$ kg/m^3 and $\nu = 10^{-6}$ m^2/s. The dimensional vortex parameters were $B_0 = 45$ cm^2/s, $2b_0 = 15$ cm, and $r_0 = 3$ cm ($r_c = 0.2$). For these parameters, $Re = 4.5 \times 10^3$. The horizontal and vertical resolutions were 1.5 cm ($L = 192$ cm, $N = 64$), and the damping parameters were $D_0 = 100$, $n^* = 26$, and $\Delta n = 4$. The initial energy was thus concentrated in wave numbers $n < 22$, which corresponds to scales > 9 cm. The vortices were initially located at a height 30 cm above the bottom of the solution domain, and the signs of the circulations were chosen so that the vortex pair would rise. Rising rather than descending vortices were used because we frequently compare our numerical results to results from laboratory experiments where rising vortices are generally more convenient to generate.[12,21–23,42] After 22 s, the vortices had risen 61.5 cm and had lost only 3% of their initial energy. As pointed out in Sec. III, this rise height agrees quite well with laboratory observations. We thus conclude that the damping specified above does not have an adverse impact on the computed vortex evolution.

In the remainder of this paper, we will use the preceding vortex pair in a variety of environments to study the effect of the environment on vortex evolution. Except where noted, the vortex-pair characteristics, the resolution, and the damping parameter values used above are kept constant in subsequent calculations, and the ambient stratification and shear are varied. As in the preceding discussion, we chose the working fluid to be water.

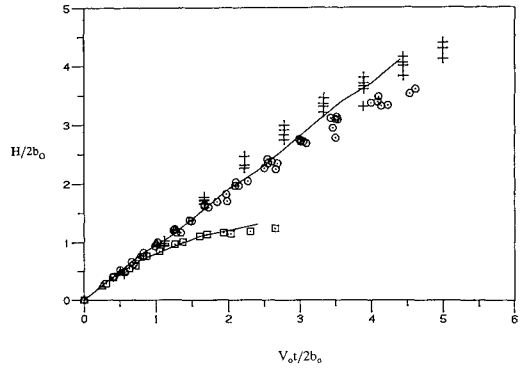

Fig. 1 Vortex rise height as a function of time for several laboratory data sets [infinite Froude number data are from Barker and Crow[21] (triangles), Tomassian[22] (plus symbols), Sarpkaya and Johnson,[12] and Sarpkaya[23] (circles); squares represent data for Froude number unity from Sarpkaya and Johnson[12] and Sarpkaya[23]; the two solid curves are our numerical results for Froude numbers infinity (top curve) and unity (bottom curve); mean shear is zero in all cases].

III. Comparison of Numerical and Laboratory Vortex Migration Results

As a test of the numerics, we compared the evolution of vortex pairs from our numerical model to results previously reported in controlled laboratory experiments. Because no experimental observations of vortex evolution in sheared flows have been reported, the comparisons are in nonsheared flows.

In experimental flows, the vortex migration Froude number is defined by

$$F_r = \frac{V_0}{N_0(2b_0)} \tag{29}$$

where F_M, given by Eq. (21), uses the ideal rise rate, $B_0/2b_0$. Barker and Crow[21] examined the motion of two-dimensional line vortex pairs in a nonstratified, nonsheared flow ($F_r = \infty$). Although Barker and Crow[21] were particularly interested in the interaction of a vortex pair with a ground plane, they show some data taken before that interaction occurs. These data are shown as the triangles in Fig. 1, which show the nondimensional vortex rise rate, $V_0t/2b_0$, vs nondimensional rise height, $H/2b_0$.

Tomassian[22] used a vortex generator similar to that of Barker and Crow[21] to study two-dimensional vortex pairs in both nonstratified and stratified flows. The stratifications used by Tomassian were such that the vortex Froude number varied from infinity to two. Nondimensional data from the nonstratified experiments ($F_r = \infty$) from Tomassian[22] are shown as the plus symbols in Fig. 1.

Sarpkaya and Johnson[12] and Sarpkaya[23] used an airfoil in a towing tank to study three-dimensional trailing vortices. In their experiments, the Froude number ranged from infinity to one. Their data are shown in Fig. 1 as the circles ($F_r = \infty$) and the squares ($F_r = 1$). The stratified data show a smaller vortex rise than the nonstratified data, a result also shown by Tomassian.[22]

The two solid curves in Fig. 1 are the vortex rise results from our numerical model for Froude numbers of infinity (top curve) and one (bottom curve). In this figure and in the remainder of this paper, the heights of the vortex cores in the numerical simulations are defined as the heights of local extrema in the perturbation vorticity field. The stratification used for the Froude number unity case was $N_0 = 0.2\ \mathrm{s}^{-1}$. Note that the Froude number infinity case was first presented at the end of Sec. II.

The results in Fig. 1 indicate that the numerically obtained vortex rise heights agree well with the experimental observations. The good agreement shown in Fig. 1 is important since the experimentally generated vortices were distinctly turbulent, whereas the damping model used in the numerical model is ad-hoc and is not meant to model rigorously the turbulent flowfield. It thus appears that generated turbulence may not be a major influence on vortex trajectories. Other numerical simulations we have performed (not shown) of vortices from Boeing 747 aircraft also show good agreement between the predicted vortex height vs time and observations. In these simulations, Re was 7×10^6.

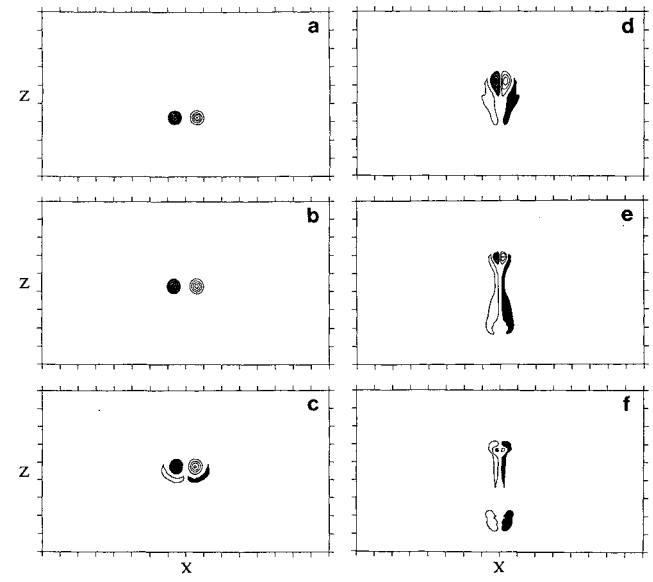

Fig. 2 Contours of perturbation vorticity η' at nondimensional times 0, 1, 2, 3, 4, and 5 (a through f, respectively), for the no-shear case $Ri = \infty$, $F_M = 1$, $F_S = \infty$ [white (black) shading signifies clockwise (counterclockwise) vorticity; contour interval is $\eta' T_0 = 10$, and each tic interval represents $0.8L_0$; the computational domain is $12.8L_0$ by $8L_0$ ($12.8L_0$ by $7.2L_0$ shown)].

IV. Results Illustrating Shear Effects

We now examine the dynamics of vortices in stratified fluids first without and then with shear. Our main objective is to show the dramatic effect that shear has on the evolution of vortices in a stratified fluid.

The temporal evolution of the vortex dynamics can be presented using any one of four time scales. The first scale is dimensional time, t, as would be observed in the laboratory. The second time scale is fractions of a B-V period, or $N_0t/2\pi$, where the B-V period is $2\pi/N_o$. The third time scale is fractions of a shear period, or $U_zt/2\pi$, where the shear period is $2\pi/U_z$. The fourth time scale is fractions of the scaling time T_0 or $\bar{t} = t/T_0$. To allow us to nondimensionally compare all of our simulations, including those in nonstratified ($N_0 = 0$) and nonsheared ($U_z = 0$) flows, we will present our results using the last time scale. For the vortices used here, $T_0 = 5$ s (cf. Sec. II).

We begin by showing results from the Froude number unity, no-shear case ($Ri = \infty$, $F_M = 1$, $F_S = \infty$) of Sec. III. Figures 2 and 3 show the computed fields of perturbation vorticity η' and total density $\bar{\rho} + \rho'$, respectively, for nondimensional times, $\bar{t} = 0,1,2,3,4,5$ (the B-V period is 6.28 time units). An important feature of these plots is the left-right symmetry of the flowfield as the regions containing vorticity rise and subsequently fall due to the effect of buoyancy. Vortices rise as time increases from 0–3 time units, at which point the heavy fluid which has been advected upward begins to fall, leaving behind a residual vortex pair which continues to rise but which ceases to be the dominant feature in the flow. At this time, light fluid begins to be advected downward. Motion associated with falling fluid is the dominant flow feature for times after 3 time units.

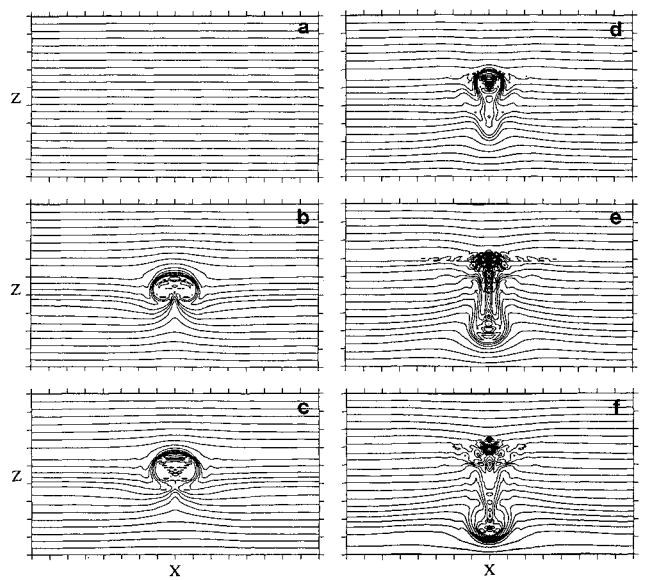

Fig. 3 Contours of total density $\rho + \rho'$ at nondimensional times 0, 1, 2, 3, 4, and 5 [(a through f, respectively), for the no-shear case $Ri = \infty$, $F_M = a$, $F_S = 1$; contour interval is $0.00033R_0$ gm/cm^3; each tic interval represents $0.8L_0$; the computational domain is $12.8L_0$ by $8L_0$ ($12.8L_0$ by $7.2L_0$ shown)].

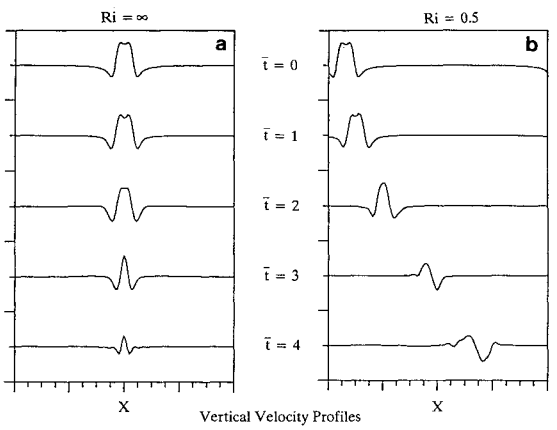

Fig. 4 Vertical velocity profiles along a horizontal line through the clockwise vortex for a) $Ri = \infty$ and b) $Ri = 0.5$ (profiles are shown for nondimensional times 0, 1, 2, 3, 4 and extend across the entire computational domain; one vertical tic represents a speed of $6.67U_0$).

Also evident in Fig. 2, is the counter-sign vorticity that is generated below the primary vortices as they rise in the stratified fluid. This vorticity generation is actually ocurring at $\bar{t} = 1$ (part b of Fig. 2), but is not visible until $\bar{t} = 2$ (part c of Fig. 2) because the vorticity magnitude represented by the lowest vorticity contour level in part b of Fig. 2 ($\eta' T_0 = 5$) is greater than the peak magnitude of counter-vorticity occurring there ($\eta' T_0 = 3.5$). The effect of mutual straining of primary and counter-vorticity regions provides another explanation of the flow evolution depicted in Fig. 2.

A third way to understand the flow evolution is to examine a time sequence of the vertical velocity along a horizontal line through the center of the major clockwise vortex. A sequence for this case is shown in part a of Fig. 4, where the gradual weakening of the primary vortex pair is quite evident.

Energy diagnostics are shown in Figs. 5 and 6. Figure 5 shows the horizontally summed total, kinetic, and potential perturbation energy density vs height for $\bar{t} = 0,1,2,3,4$, and 5. In this figure, the energy density peak associated with the vortices rises for about 3 time units after which there is a

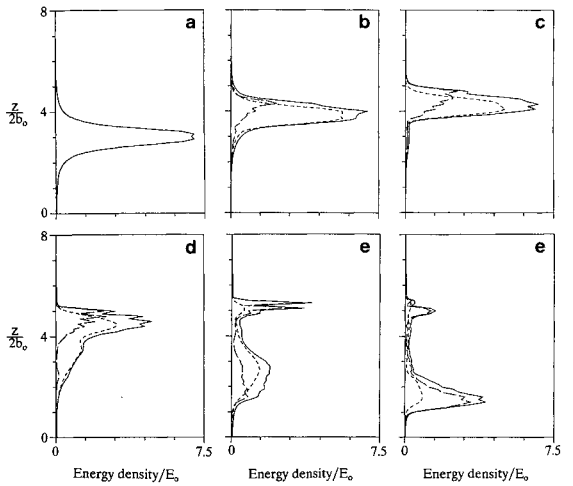

Fig. 5 Vertical profiles of horizontally summed perturbation energy density for nondimensional times 0, 1, 2, 3, 4 and 5 (a through f, respectively) for the no-shear case $Ri = \infty$, $F_M = 1$, $F_S = \infty$ (solid, short-dash, and long-dash lines signify total, kinetic, and potential perturbation energy density, respectively).

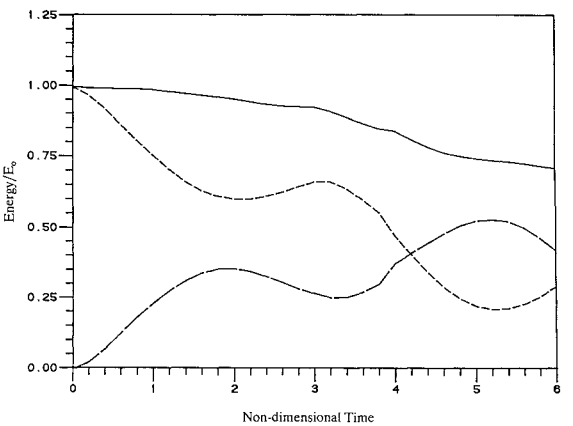

Fig. 6 Perturbation energy vs time for the no-shear case $Ri = \infty$, $F_M = 1$, $F_S = \infty$ (solid, short-dash, and long-dash lines signify total, kinetic, and potential perturbation energy, respectively).

descending energy density peak which becomes dominant. A residual energy density peak remains at the upper level but becomes insignificant at later times.

Plots of total, kinetic, and potential perturbation energy vs time are shown in Fig. 6. The initial increase in potential energy and decrease in kinetic energy are associated with the initial rise of the vortices. There is then a slight decrease in potential and increase in kinetic energy as fluid begins to be advected downward and a pair of descending vorticity regions begins to form. As these new regions fall, carrying fluid with them, potential energy resumes increasing and kinetic energy decreases until about $\bar{t} = 5.3$. In the meantime, total perturbation energy has decreased about 25% as smaller scales of motion are damped out. At 6 time units, the computed flowfield shows a tendency toward equipartition of potential and kinetic energy, as we expect, since the flow is evolving into an internal wave field.

The preceding results for the nonsheared, Froude number unity case show a left/right symmetry and a rise and fall of the perturbation energy density peak with time. When a mean current with uniform shear is imposed on the preceding flow, the outcome is dramatically different. We first consider the case $Ri = 0.5$ ($F_M = 1$, $F_S = 0.7$). The mean velocity we specify is zero at the bottom boundary and toward the right at the top boundary (clockwise rotation). Figures 7 and 8 are analagous

to Figs. 2 and 3 for the no-shear case. The initial perturbation vorticity (part a of Fig. 7) and total density (part a of Fig. 8) are identical to those shown in part a of Figs. 2 and 3, respectively.

In this flow, as time increases, Fig. 7 shows that the counterclockwise vortex is gradually destroyed so that the induced velocity acting on the right vortex becomes weaker than that on the left. The unequal stengths of the left and right vortices result in a tilt of the vortex system, i.e., the line joining the cores of the left and right vortices is no longer horizontal. Tilting of the vortex system has been observed in aircraft trailing vortices.[2,5] By $\bar{t}=3$, the vorticity has evolved into a single solitary feature plus weak remnants. This solitary feature maintains its identity for the duration of the calculation. Note the slow decay of the solitary vortex as evidenced by the slow change in the number of contours inside the clockwise (white) vortex.

Evident in Fig. 7, as it was in Fig. 2, is the formation of countersign vorticity below the primary vortices. Analogous to what we noted in our discussion of Fig. 2, our choice of vorticity contour levels results in generated vorticity not being visible in part b of Fig. 7 nor beneath the clockwise vortex in part c of Fig. 7. In fact, the nondimensional magnitude of peak counter-vorticity below the clockwise vortex in part c of Fig. 7 is 4.0 and below the counterclockwise vortex it is 6.6; as before, the magnitude of the lowest contour level is 5. The mutual straining of the various vorticity regions again provides an alternate explanation of the flow evolution.

In Fig. 8, the density plots show an initial upward advection of heavy fluid, similar to the no-shear case shown in Fig. 3. In contrast to the no-shear case, however, here there is no significant downward advection of fluid after $\bar{t}=3$. Instead, the major disturbance remains significantly higher than the initial height of the vortex pair, the height varying slightly with time due to the effect of stratification.

Figures 7 and 8 indicate the dramatic effect of shear on the evolution of the vortex pair in a stratified flow. Without shear, the vortices evolved symmetrically, losing their individual identities equally rapidly. With shear, the vortex with rotation in opposition to the rotational sense of the mean shear is destroyed, and the vortex with rotation in the same sense as the mean shear survives. In this case, a solitary vortex is formed, and it decays slowly with time.

Vertical velocity profiles for the $Ri=0.5$ case are shown in part b of Fig. 4; they contrast sharply with those shown in part a of Fig. 4 for the preceding, no-shear case. This time we see a clear transition from a vortex-pair profile to a profile of a single vortex.

Figure 9 shows the horizontally summed perturbation energy density vs height plots for the $Ri=0.5$ case. These plots show that the energy density peak at late times remains near the level achieved during the first 2 time units instead of falling below the starting ($\bar{t}=0$) level, as in the no-shear case. Also, the ratio of kinetic to potential energy density is greater at late times than it was for the no-shear case. In the perturbation energy vs time plots in Fig. 10, the potential energy initially increases as in the no-shear case, but at $\bar{t}=3$, instead of continuing to rise, it begins a monotonic decrease. This decrease begins around the same time the solitary vortex is formed. There is also no longer a trend toward equipartition of the kinetic and potential perturbation energy at late times. For times $\bar{t}>3$, the shear maintains the integrity of the clockwise vortex and prevents the downward transport of fluid. This results in less energy being transformed into internal gravity waves and a dominance of kinetic over potential per-

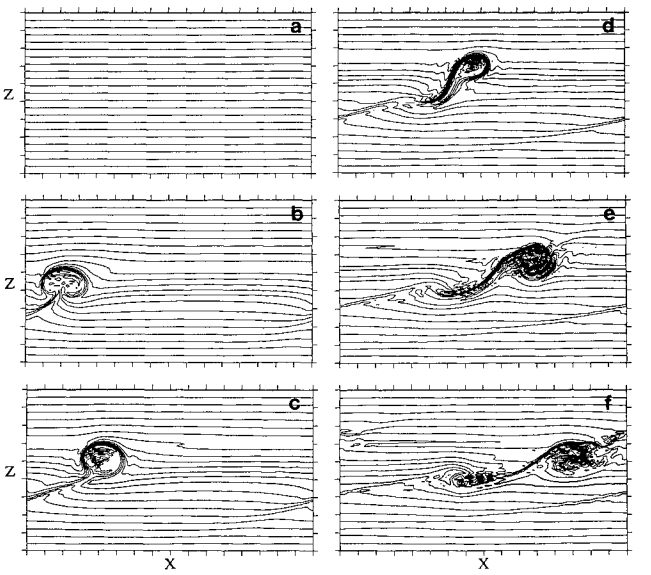

Fig. 8 As in Fig. 3 for the high-shear case, $Ri=0.5$, $F_M=1$, $F_S=0.7$ (the computational domain is $12.8L_0$ by $7.2L_0$).

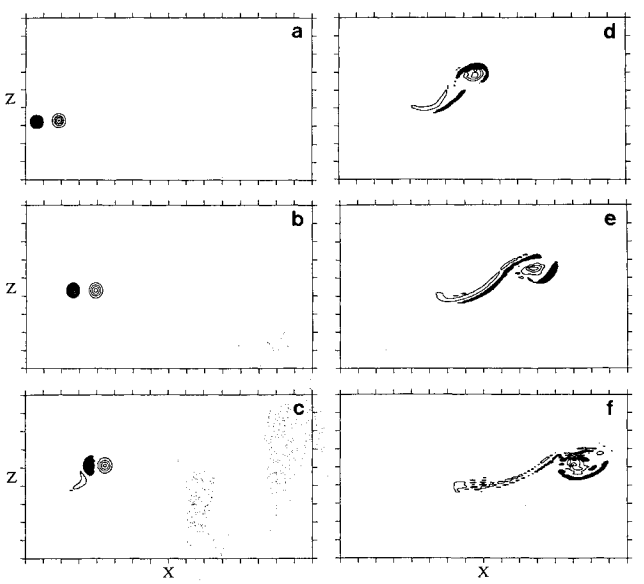

Fig. 7 As in Fig. 2 for the high-shear case, $Ri=0.5$, $F_M=1$, $F_S=0.7$ (the computational domain is $12.8L_0$ by $7.2L_0$).

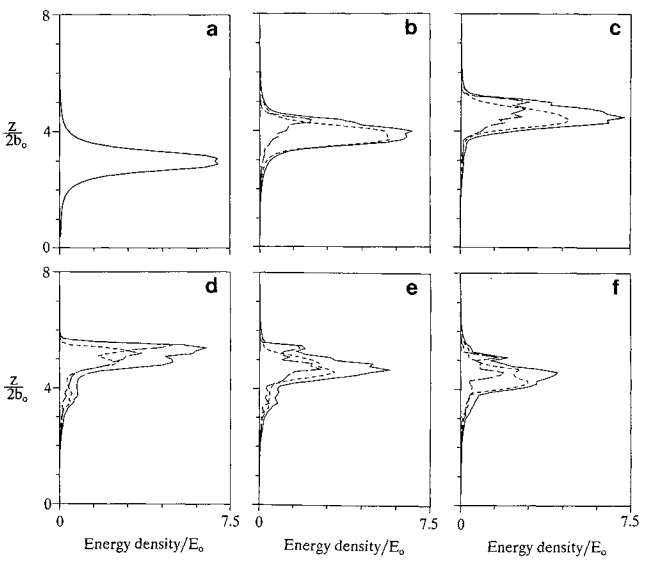

Fig. 9 As in Fig. 5 for the high-shear case, $Ri=0.5$, $F_M=1$, $F_S=0.7$.

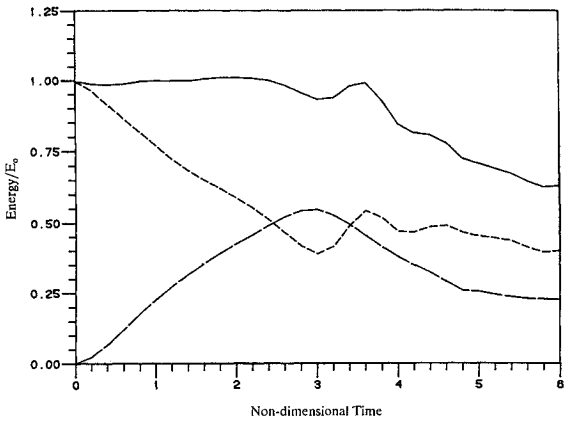

Fig. 10 As in Fig. 6 for the high-shear case, $Ri = 0.5$, $F_M = 1$, $F_S = 0.7$.

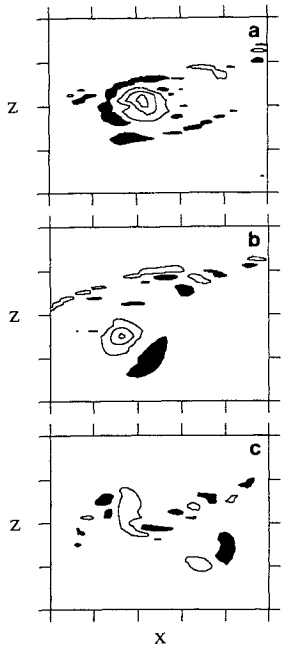

Fig. 11 Contours of perturbation vorticity η' for $F_M = 1$ and $t = 6$ [white (black) shading signifies clockwise (counterclockwise) vorticity; contour interval is $\eta' T_0 = 10$, and each tic interval represents $0.8L_0$; a) $Ri = 0.5$, $F_S = 0.7$; b) $Ri = 1$, $F_S = 1$; c) $Ri = 4$, $F_S = 2$].

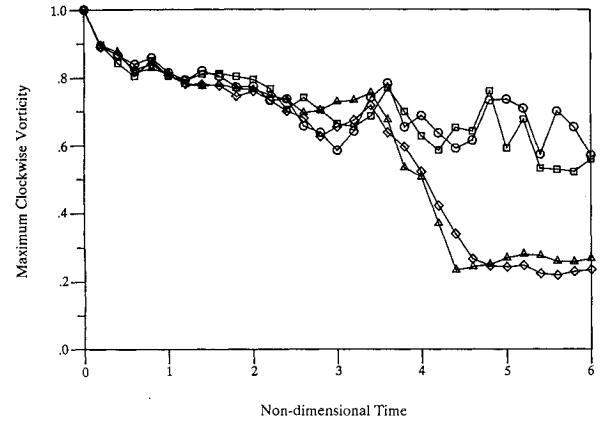

Fig. 12 Ratio of the maximum clockwise vorticity to the initial maximum clockwise vorticity vs time for four numerical simulations with $F_M = 1$ [circles are for the case $Ri = 0.5$ ($F_S = 0.7$), squares for $Ri = 1$ ($F_S = 1$), triangles for $Ri = 4$ ($F_S = 2$), and diamonds for $Ri = \infty$ ($F_S = \infty$)].

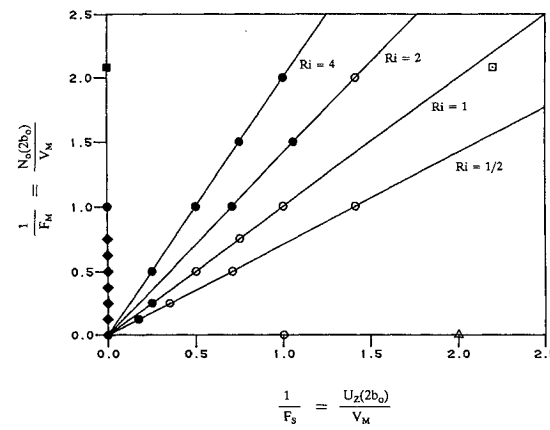

Fig. 13 Summary data plot [open (solid) symbols denote the occurrence (nonoccurrence) of a solitary vortex at a simulation time of one B-V period; the circles are our numerical results; the squares are for the numerical/experimental results of Delisi et al.[42]; the triangle represents the numerical calculation of Bilanin et al.[30]; diamonds and the closed circles on the vertical axis signify the experimental results of Barker and Crow,[21] Tomassian,[22] Sarpkaya and Johnson,[12] and Sarpkaya[23]; the horizontal and vertical axes represent reciprocals of the shear and stratification parameters defined by Eqs. (22) and (21), respectively; solid lines are constant Richardson number loci.

turbation energy. The brief increase in total and kinetic perturbation energy near $\bar{t} = 3.6$ arises from a momentary increase in the rate that energy is transferred toward small scales.

V. Further Results and Discussion

We have seen that the presence of strong shear can have a dramatic effect on the evolution of a vortex pair in a stratified fluid. The preceding results were obtained for flows having Froude number unity. We now consider the effect of a weaker shear and the effect of varying the Froude number.

Figure 11 illustrates the effect of Richardson number on the evolution of a solitary vortex for the Froude number unity case. Here, we show contour plots of perturbation vorticity for Richardson numbers of a) 0.5, b) 1, and c) 4 at a time of 6 units (about 1 B-V period). Part a of Fig. 11 is a continuation of the evolution shown in Fig. 7.

Figure 11 shows that a distinct, solitary vortex has developed in both the $Ri = 0.5$ and 1 cases. In these flows, the bulk of the clockwise vorticity is organized into a single vortex, and this solitary vortex is significantly stronger (i.e., has many more contour levels) than the counterclockwise vorticity. In contrast, the $Ri = 4$ case shows that the maximum clockwise vorticity is nearly the same strength as the maximum counterclockwise vorticity. In this case, both vortices are decaying at about the same rate, and a solitary vortex has not formed.

Figure 12 shows, as a function of time, the ratio of the maximum clockwise vorticity to the initial maximum clockwise vorticity for the cases with $Ri = 0.5$, 1, 4, and infinity, with $F_M = 1$. The maximum clockwise vorticity is used here as an indication of the strength of the clockwise vortex. In this figure, we see that the decay is similar in all cases up to a time of about 3.4 units (about one-half B-V period). At this time, the maximum clockwise vorticity for the $Ri = \infty$ case begins to decrease rapidly. This decrease corresponds to the time when motion associated with falling fluid becomes the dominant flow feature. A similar decay is observed for the $Ri = 4$ case. For the high-shear cases, $Ri = 1$ and 0.5, the decay rates are slow and nearly constant up to the end of the numerical simulation. It is for these two cases that we observed solitary vortices.

An additional calculation showed nonsolitary evolution for $Ri = 2$. Thus, for $F_M = 1$, there appears to be a transition

Richardson number between one and two with different flow regimes on either side. In flows with a Richardson number of two or greater, a solitary vortex does not develop, and the maximum clockwise vorticity decays essentially the same as in the no-shear case. When the Richardson number is one or less, a solitary vortex develops, and that vortex decays slowly.

Additional calculations were performed to estimate transition Richardson numbers for other Froude numbers. A plot which includes a summary of all our results is shown in Fig. 13. Here, the vertical axis represents flows with stratification and no shear, the horizontal axis represents flows with shear and no stratification, and the origin corresponds to flows with no stratification and no shear. Straight lines through the origin are lines of constant Richardson number. Open symbols denote cases for which a solitary vortex formed, and solid symbols represent cases for which a solitary vortex did not form.

Our numerical calculations are indicated by circles. A vortex pair evolution was declared solitary (open circles) if the final maximum clockwise vorticity exceeded the final minimum counterclockwise vorticity by more than 40% of the counterclockwise value, and nonsolitary (solid circles) if this percentage was less than 25. Evolutions thus declared solitary behaved qualitatively as the previous $Ri = 0.5$ and 1.0, $F_M = 1.0$ cases, and those declared nonsolitary behaved qualitatively as the previous $Ri = 4.0$, $F_M = 1$ case. All determinations of solitary or nonsolitary were made at a simulation time of one B-V period. This is an important point, for in at least one case ($Ri = 4$ and $F_M = 0.5$), a nonsolitary evolution at a time of one B-V period became solitary at two B-V periods. Note, that due to buoyancy effects, not all nonsolitary outcomes become solitary as evolution time increases.

The two squares in Fig. 13 represent results from Delisi et al.[42] Each square denotes both a numerical and a laboratory experiment; in both cases the numerical and laboratory results were in agreement. The determination of solitary or nonsolitary for these two cases was done at one third of a B-V period, which was the run time of the experiments.

Also shown in Fig. 13 are the numerical and experimental results of vortex evolution reported by previous investigators. The open triangle in Fig. 13 represents the numerical calculation of Bilanin et al.[30] A similar numerical calculation by Rossow,[29] in a flow with shear but no stratification, is on the horizontal axis but off scale. Results of Barker and Crow,[21] Tomassian,[22] Sarpkaya and Johnson,[12] and Sarpkaya[23] are shown either as the closed diamonds or as the closed circles on the vertical axis. (The closed circles on the vertical axis represent both our numerical calculations and previous experimental results.) Note that previous results fall only along either the horizontal or vertical axes. Thus, previous studies are special cases of the more general results presented here.

From Fig. 13, we see that the transition between nonsolitary and solitary vortex evolution generally occurs over Richardson numbers between 0.5 and 4 (for Froude numbers between 0.5 and 4) with a trend toward larger transition Ri values as Froude number decreases (stratification increases). We anticipate that the transition Ri values may also vary with other parameters such as Reynolds number (we used laboratory values), vortex core size, and vortex strength. Also, recall that the $Ri = 4.0$, $F_M = 0.5$ case had a nonsolitary result for a simulation time of one B-V period and a solitary result at two B-V periods. This suggests that the transition Richardson numbers in Fig. 13 shift somewhat to the left as evolution time increases.

For cases to the left of the transition Richardson numbers, we expect that the initial vortex energy that is not dissipated due to viscosity will eventually be transformed into internal waves. For these cases, the effect of the stratification is greater than the effect of the shear, and buoyancy forces destroy unified, vortical structures. Also, an increase in stratification causes a decrease in vortex lifetime by causing energy to be transferred more rapidly into the radiating internal-wave field. For cases to the right of the transition Richardson numbers, a solitary vortex develops from the initial vortex pair, and the shear acts to maintain a single vortical structure, thus increasing vortex lifetime.

Acknowledgments

We thank George C. Greene, David C. Fritts, R. David Lucas, and Professor T. Sarpkaya for helpful and stimulating discussions. This study was supported by Northwest Research Associates, Inc., internal research and development funding and by Office of Naval Research Contract N00014-89-C-0030.

References

[1]Rossow, V. J. and Tinling, B. E., "Research on Aircraft/Vortex-Wake Interactions to Determine Acceptable Level of Wake Intensity," *Journal of Aircraft*, Vol. 25, 1988, pp. 481-492.

[2]MacCready, P. B., Jr., "An Assessment of Dominant Mechanisms in Vortex-Wake Decay," *Aircraft Wake Turbulence and Its Detection*, edited by J. H. Olsen et al., Plenum, New York, 1971, pp. 289-304.

[3]Burnham, D. C., "Effect of Ground Wind Shear on Aircraft Trailing Vortices," *AIAA Journal*, Vol. 10, 1972, pp. 1114-1115.

[4]Burnham, D., Hallock, J., Kochs, R., and Sullivan, T., "Vortex Sensing Tests at NAFEC," U.S. Dept. of Transportation, Federal Aviation Administration, Rept. DOT-TSC-FAA-72-2, 1972.

[5]Tombach, I. H., "Observations of Atmospheric Effects on Vortex Wake Behavior," *Journal of Aircraft*, Vol. 10, 1973, pp. 641-647.

[6]Tombach, I. H., "Influence of Meteorological Factors on the Vortex Wake of a Light Twin-Engine Aircraft," AeroVironment, Inc., Pasadena, CA, Rept. AV-FR-416, 1974.

[7]Brashears, M. R., Logan, N. A., and Hallock, J. N., "Effect of Wind Shear and Ground Plane on Aircraft Wake Vortices," *Journal of Aircraft*, Vol. 12, 1975, pp. 830-833.

[8]Burnham, D. C., "B-747 Vortex Alleviation Flight Tests: Ground-Based Sensor Measurements," U.S. Dept. of Transportation, Federal Aviation Adminstration, Rept. DOT-FAA-RD-81-99, 1982.

[9]Hill, F. M., "A Numerical Study of the Descent of a Vortex Pair in a Stably Stratified Atmosphere," *Journal of Fluid Mechanics*, Vol. 71, 1975, pp. 1-13.

[10]Hecht, A. M., Bilanin, A. J., Hirsch, J. E., and Snedeker, R. S., "Turbulent Vorticies in Stratified Fluids," *AIAA Journal*, Vol. 18, 1980, pp. 738-746.

[11]Hecht, A. M., Bilanin, A. J., and Hirsch, J. E., "Turbulent Trailing Vortices In Stratified Fluids," *AIAA Journal*, Vol. 19, 1981, pp. 691-698.

[12]Sarpkaya, T. and Johnson, S. K., "Trailing Vortices in Stratified Fluids," Naval Postgraduate School, Monterey, CA, Rept. NPS-69-82-003, 1982.

[13]Crow, S. C., "Stability Theory for a Pair of Trailing Vortices," *AIAA Journal*, Vol. 8, 1970, pp. 2172-2179.

[14]Scorer, R. S. and Davenport, L. J., "Contrails and Aircraft Downwash," *Journal of Fluid Mechanics*, Vol. 43, 1970, pp. 451-464.

[15]Saffman, P. G., "The Motion of a Vortex Pair in a Stratified Atmosphere," *Studies in Applied Math*, Vol. 51, 1972, pp. 107-119.

[16] Crow, S. C., "Motion of a Vortex Pair in a Stratified Fluid," Poseidon Research, Santa Monica, CA, Rept. 1, 1974.

[17]Greene, G. C., "An Approximate Model of Vortex Decay in the Atmosphere," *Journal of Aircraft*, Vol. 23, 1986, pp. 566-573.

[18]Olsen, J. H., "Results of Trailing Vortex Studies in a Towing Tank," *Aircraft Wake Turbulence and Its Detection*, edited by J. H. Olsen et al., Plenum, New York, 1971, pp. 455-472.

[19]Baker, G. R., Barker, S. J., Bofah, K. K., and Saffman, P. G., "Laser Anemometer Measurements of Trailing Vortices in Water," *Journal of Fluid Mechanics*, Vol. 65, 1974, pp. 325-336.

[20]Maxworthy, T., "Some Experimental Studies of Vortex Rings," *Journal of Fluid Mechanics*, Vol. 81, 1977, pp. 465-495.

[21]Barker, S. J. and Crow, S. C., "The Motion of Two-Dimensional Vortex Pairs in a Ground Effect," *Journal of Fluid Mechanics*, Vol. 82, 1977, pp. 659-671.

[22]Tomassian, J. D., "The Motion of a Vortex Pair in a Stratified Medium," Ph.D. Dissertation in Engineering, University of California at Los Angeles, 1979.

[23]Sarpkaya, T., "Trailing Vortices in Homogeneous and Density-Stratified Media," *Journal of Fluid Mechanics*, Vol. 136, 1983, pp. 85-109.

[24]Hall, M. G., "Vortex Breakdown," *Annual Reviews of Fluid Mechanics*, Vol. 4, 1972, pp. 195-218.

[25]Widnall, S. E., "The Structure and Dynamics of Vortex Filaments," *Annual Reviews of Fluid Mechanics*, Vol. 7, 1975, pp. 141–165.

[26]Leibovich, S., "The Structure of Vortex Breakdown," *Annual Reviews of Fluid Mechanics*, Vol. 10, 1978, pp. 221–246.

[27]Saffman, P. G. and Baker, G. R., "Vortex Interactions," *Annual Reviews of Fluid Mechanics*, Vol. 11, 1979, pp. 95–122.

[28]Smith, J. H. B., "Vortex Flows in Aerodynamics," *Annual Reviews of Fluid Mechanics*, Vol. 18, 1986, pp. 221–242.

[29]Rossow, V. J., "Convective Merging of Vortex Cores in Lift-Generated Wakes," AIAA Paper 76-415, July 1976.

[30]Bilanin, A. J., Teske, M. E., and Hirsch, J. E., "Neutral Atmospheric Effects on the Dissipation of Aircraft Vortex Wakes," *AIAA Journal*, Vol. 16, 1978, pp. 956–961.

[31]Eriksen, C. C., "Measurements and Models of Fine Structure, Internal Gravity Waves, and Wave Breaking in the Deep Ocean," *Journal of Geophysical Research*, Vol. 83, 1978, pp. 2989–3009.

[32]Evans, D.L., "Observations of Small-Scale Shear and Density Structure in the Ocean," *Deep-Sea Research*, Vol. 29, 1982, pp. 581–595.

[33]Toole, J. M. and Hayes, S. P., "Finescale Velocity-Density Characteristics and Richardson Number Statistics of the Eastern Equatorial Pacific," *Journal of Physical Oceanography*, Vol. 14, 1984, pp. 712–726.

[34]Mahrt, L., Heald, R. C., Lenschow, D. H., Stankov, B. B., and Troen, I., "An Observational Study of the Structure of the Nocturnal Boundary Layer," *Boundary-Layer Meteorology*, Vol. 17, 1979, pp. 247–264.

[35]Barat, J., "The Fine Structure of the Stratospheric Flow Revealed by Differential Sounding," *Journal of Geophysical Research*, Vol. 88, 1983, pp. 5219–5228.

[36]Mahrt, L., "Vertical Structure and Turbulence in the Very Stable Boundary Layer," *Journal of the Atmospheric Sciences*, Vol. 42, 1985, pp. 2333–2349.

[37]Fritts, D. C., "The Nonlinear Gravity Wave-Critical Level Interaction," *Journal of the Atmospheric Sciences*, Vol. 35, 1978, pp. 397–413.

[38]Fritts, D. C., "The Excitation of Radiating Waves and Kelvin-Helmholtz Instabilities by the Gravity Wave-Critical Level Interaction," *Journal of the Atmospheric Sciences*, Vol. 36, 1979, pp. 12–23.

[39]Fritts, D. C., "The Transient Critical-Level Interaction in a Boussinesq Fluid," *Journal of Geophysical Research*, Vol. 87, 1982, pp. 7997–8016.

[40]Dunkerton, T. J. and Fritts, D. C., "Transient Gravity Wave-Critical Layer Interaction. Part I: Convective Adjustment and the Mean Zonal Acceleration," *Journal of the Atmospheric Sciences*, Vol. 41, 1984, pp. 992–1007.

[41]Roache, P. J., *Computational Fluid Dynamics*, Hermosa, Albuquerque, NM, 1976, p. 61.

[42]Delisi, D. P., Robins, R. E., and Lucas, R. D., "Laboratory Observations of the Effect of Shear on the Evolution of a Vortex Pair in a Stratified Fluid," in preparation.